RSC Advances

ROYAL SOCIETY OF CHEMISTRY

www.rsc.org/advances

Synthesis and Characterization of Thermo-responsive and Photo-cleavable Block Copolymers as Nanocarriers

Ren-Shen Lee[a,*], Shiu-Wei Wang[a], You-Chen Li[a], Jia-You Fang[b]

[a]*Division of Natural Science, Center of General Education, Chang Gung University, 259 Wen-Hwa 1st Road, Kwei-Shan, Tao-Yuan 333, Taiwan. Tel.: +886-3-2118800x5054; Fax: +886-3-2118700; E-mail: shen21@mail.cgu.edu.tw*

[b]*Graduate Institute of Natural Products, Chang Gung University, Tao-Yuan, Taiwan*

Abstract

In this study, we synthesized thermo-responsive and photo-cleavable amphiphilic block copolymers containing photodegradable linkers as junction points between hydrophilic and hydrophobic chains. We synthesized PNiPAAm-ONB-PXCL block copolymers by using a combination of ring-opening polymerization and nucleophilic substitution reactions using 5-hydroxy-2-nitrobenzyl alcohol as a difunctional photo-responsive initiator. These PNiPAAm-ONB-PXCL copolymers consisting of soft domains of amorphous PNiPAAm and PXCL, exhibited amorphous T_g. The polymer micelles exhibited dual responsiveness to heat and light. The lower critical solution temperature of $PNiPAAm_{20}$-ONB-$PMCL_{49}$ was 39.3 ℃, which is approximately the temperature of tumor tissue. When we exposed the polymer solutions to ultraviolet (UV) irradiation, we observed major changes in the structure and morphology of the particles. Fluorescence emission measurements indicated the release of Nile red (NR), a hydrophobic dye, encapsulated by the PNiPAAm-ONB-PXCL micelles, in response to irradiation because of disruption of the micelles. Release of indomethacin (IMC) was rapid under UV irradiation at 42 ℃ and approximately 90% of the encapsulate IMC was released in a sustained manner during the first 7 h. The nanoparticles were associated with nonsignificant toxicity at concentrations $<$ 100 μg mL^{-1}. Doxorubicin (DOX)-loaded micelles facilitated the

uptake of DOX by HeLa cells within 30 min of treatment, and were predominantly retained in the cytoplasm. The DOX-loaded micelles were associated with low cytotoxicity against HeLa cells.

Keywords: amphiphilic, thermo-responsive, photo-cleavable, o-nitrobenzyl alcohol, cellular uptake

Introduction

Amphiphilic block copolymers (BCPs) have attracted considerable attention for applications in various fields such as controlled drug delivery, nano-reactors, or biomimetics [1-4]. Nanostructures such as micelles, nanospheres and vesicles, -among others, can be formed through the self-assembly of amphiphilic copolymers in water. Polymeric micelles are composed of a core containing hydrophobic blocks and a corona or shell of the hydrophilic blocks. The incorporation of stimuli-responsive moieties within polymers renders them potentially useful as controlled delivery systems [5-7].

Various types of stimuli such as pH [8-10], temperature [11-12], light irradiation [13-14], and redox [15-16], can be used to modulate block copolymer assembly. Previous studies have widely investigated polymeric micelles, which exhibit dual responsiveness, using light and temperature as external stimuli [17-24]. Light is a particularly useful external trigger because it allows precise temporal (when the light source is switched on) and spatial (where the light is directed to) control. Temperature is another useful environmental trigger of the formation and dissociation of micelles. Despite a broad range of possible applications for polymeric micelle systems, suitable thermo-responsive and photo-dissociable polymer structures remain limited. Several groups have applied an approach based on using a photo-cleavable junction to link hydrophilic and hydrophobic blocks [25-28]. After micelle formation, light can be applied to break block copolymer chains at the junction point. Among the investigated photolabile groups, o-nitrobenzyl alcohol (ONB) derivatives have received considerable attention in the field of synthetic polymer and material science [29-31].

In this study, we synthesized an easily cleavable poly(N-isopropyl acrylamide)-ONB-poly(4-substituted- ε -caprolactone) (PNiPAAm-ONB-PXCL) by using UV irradiation, in which a photochemical sensitive ONB group was installed as

a linker. PNiPAAm is one of the most responsive of the thermo-responsive polymers, which have a lower critical solution temperature (LCST), defined as the critical temperature below which an aqueous polymer solution undergoes a phase transition from a soluble to an insoluble state [32]. PXCL is an amorphous, biocompatible and biodegradable polyester [33]. In this study, we synthesized the desired amphiphilic ONB-linked PNiPAAm-b-PXCL copolymers, PNiPAAm-ONB-PXCL, with PNiPAAm as a hydrophilic block and poly(4-methyl- ε -caprolactone) (PMCL), or poly(4-phenyl- ε -caprolactone) (PBCL) as a hydrophobic block, by using ring-opening polymerization (ROP) and nucleophilic substitution reactions. To the best of our knowledge, the thermo-responsive and photo-cleavable PNiPAAm-ONB-PXCL copolymers have never been investigated. We also investigated the influence of hydrophilic and hydrophobic chain lengths of block copolymers on micelle size, drug entrapment efficiency, and drug-loading content. We examined the physicochemical and photodegradable properties of these micelles in aqueous phase by using fluorescence spectroscopy, dynamic light scattering (DLS), and transmission electron microscopy (TEM). Fluorescent imaging and cytotoxicity analyses of the internalization of polymeric micelles encapsulating doxorubicin (DOX) into human cervical cancer (HeLa) cells suggested that the polymer could be useful as a carrier for drugs.

Experimental section

Materials

4-Methylcyclohexanone, 4-phenylcyclohexanone, N-isopropyl acrylamide (NiPAAm), 2-mercaptoethanol, benzoyl peroxide, pyrene, indomethacin (IMC), and Nile red (NR) were purchased from Aldrich Chemical Co. (Milwaukee, WI). *m*-Chloroperoxybenzoic acid was purchased from Fluka Chemical Co. (Buchs SG1, Switzerland). Stannous octoate ($SnOct_2$) was purchased from Strem Chemical Inc

(Newburyport, MA). NiPAAm (97%) was recrystallized twice from hexane and dried under vacuum prior to use. PNiPAAm, toluenesulfonyl-PNiPAAm (PNiPAAm-OTs), 4-methyl- ε -caprolactone (MCL) and 4-phenyl- ε -caprolactone (BCL) were prepared according to methods described previously with modifications [34-36]. Doxorubicin hydrochloride (99%) (Aldrich, Saint Louis, MO) was deprotonated to obtain hydrophobic DOX as described previously [37]. N.N-Dimethyl formamide (DMF), and toluene were distilled under calcium hydride. Other high-pressure liquid chromatography (HPLC) grade solvents, such as tetrahydrofuran (THF), dimethylsulfoxide (DMSO), methanol, chloroform ($CHCl_3$), and *n*-hexane, were purchased from Merck (Darmstade, Germany). A Milli-Q Plus system (Waters, Milford, MA) was used to obtain ultrapure water. Dulbecco's modified Eagle's medium (DMEM), trypsin/EDTA, 100× antibiotic-antimycotic, and Hoechst 33342 nuclei dye were purchased from Gibco, Invitrogen Corp. (Carlsbad, CA). Fetal bovine serum (FBS) was obtained from Biological Industry (Kibbutz Beit Haemek, Israel). A CellTiter 96® AQueuous One Solution kit was obtained from Promega (Fitchburg, Wisconsin) Amiloride, chlorpromazine, methyl-β-cyclodextrin, and nystatin were purchased from Sigma-Aldrich (St. Louis, MO).

Synthesis of PNiPAAm-ONB-PXCL diblock copolymers

All glassware was dried in an oven and handled under a dry nitrogen stream. The polymerization reaction to create $PNiPAAm_{20}$-ONB-$PMCL_{49}$ proceeded as follows: 5-hydroxy-2-nitrobenzyl alcohol (62.6 mg, 0.37 mmol), as an initiator, and MCL (2.37 g, 18.5 mmol) were introduced into a flask, heated under a dry nitrogen stream, and dissolved in 50 mL of toluene. Thirty-six milligrams of $SnOct_2$ (1.5 wt% based on the weight of ONB and MCL) were then added to the flask. The flask was purged with nitrogen and refluxed for 24 h, and the solution was vacuum-concentrated under reduced pressure. The resulting product, HONB-$PMCL_{49}$, was dissolved in $CHCl_3$,

and precipitated into excess *n*-hexane/diethyl ether (v/v 5:1) while stirring. The purified polymer was dried *in vacuo* at 50 ℃ for 24 h and analyzed. Figs. 1A and 2A show representative ^{1}H nuclear magnetic resonance (NMR) and infrared (IR) spectra of HONB-PMCL$_{49}$. The resonance peaks were assigned to the corresponding hydrogen atoms of HONB-PMCL$_{49}$. Subsequently, a mixture of HONB-PMCL$_{49}$ (0.95 g, 0.22 mmol, 1 equiv., M_n = 4250 g mol^{-1}) and potassium carbonate (92.4 mg, 0.66 mmol, 3 equiv.) was stirred in DMF (10 mL) for 1 h at 60 ℃. Toluenesulfonyl-PNiPAAm$_{20}$ (PNiPAAm$_{20}$-OTs, 0.67 g, 0.26 mmol, 1.2 equiv., M_n = 2490 g mol^{-1}) in DMF (5 mL) was added, and the mixture was stirred for 24 h at 60 ℃. DMF was removed under reduced pressure. The residue was dissolved in $CHCl_3$, and then precipitated into excess *n*-hexane/diethyl ether (v/v 5:1) while stirring. The purified polymer, PNiPAAm$_{20}$-ONB-PMCL$_{49}$, was dried *in vacuo* at 50 ℃ for 24 h and analyzed. Figs. 1B and 2C show representative ^{1}H NMR and IR spectra of PNiPAAm$_{20}$-ONB-PMCL$_{49}$.

Characterization

^{1}H NMR spectra were recorded at 500 MHz by using a Bruker WB/DMX-500 spectrometer (Ettlingen, Germany), $CHCl_3$ (δ 7.24 ppm) was used as an internal standard in chloroform-*d*. IR spectra were measured using a Bruker TENSOR 27 Fourier transform infrared (FT-IR) spectrophotometer (Bruker, Germany). Samples were placed on sodium chloride plates or pressed into potassium bromide pellets, and the number- and weight-average molecular weights (M_n and M_w, respectively) of the polymers were determined by using gel permeation chromatography (GPC). GPC was conducted using an HPLC system equipped with a model PU-2031 refractive-index detector (Jasco, Tokyo, Japan) and Jordi Gel polydivinyl benzene columns with pore sizes of 100, 500, and 1000 Å. $CHCl_3$ was used as an eluent at a flow rate of 0.5 mL min^{-1}. PEG standards of low dispersity (Polymer Sciences) were used to generate a

calibration curve. Data were recorded and manipulated using a Windows-based software package (Scientific Information Service). Thermal analysis of the polymers was performed using DSC on a DuPont 9900 system (Newcastle, DE) at a heating rate 20 ℃ min^{-1}. T_gs were read in the middle of changes in heat capacity and collected from the second heating scan after rapid cooling.

UV irradiation

The PNiPAAm-ONB-PMCL polymer (2 mg) in inhibitor-free THF (1 mL) or the micelle of polymer in PBS (0.1 M, pH 7.4) was exposed to UV light provided using a UV light system (model PR-2000, Phnchum Co., Taiwan) equipped with eight Hitachi FL8BL-B (352 nm, 8W) lamp. Samples were placed in quartz cuvettes, preferred to prevent UV absorption as from common glass vials, and irradiated at room temperature for a given amount of time, having a spot size of ~ 1 cm^2, applied vertically from the top of the cuvette.

Transmittance

Optical transmittance of the aqueous polymer solution (2 mg mL^{-1}, 0.2 wt%) at various temperatures was measured at 500 nm by using a UV-Vis spectrophotometer (Jasco V-550, Japan). The temperature of the sample cells was regulated by a temperature controller (Jasco ETC-505T, Japan). The heating rate was set at 0.1 ℃ min^{-1}. The LCST values for the polymer solutions were determined at the temperatures which optical transmittance was 50%.

Fluorescence

Fluorescence spectra were recorded using a Hitachi F-4500 fluorescence spectrometer equipped with a 20 kW xenon discharge lamp. The slit width was 10 nm and square quartz cells (1.0 × 1.0 cm) were used.

(1) Determination of critical micelle concentration (CMC). Fluorescence was evaluated using pyrene as a probe to investigate micelle formation. First, the

fluorescence spectra of pyrene were recorded in an aqueous solution at room temperature by using a fluorescence spectrophotometer. Sample solutions were then prepared by adding known amounts of pyrene in acetone to a series of flasks. After the acetone had completely evaporated, various amounts of PNiPAAm-ONB-PXCL micelle solutions at concentrations, ranging from 0.0183 to 300 mg L^{-1}, were added to each flask and mixed by vortexing. The pyrene concentration in the final solutions was 6.1×10^{-7} M. The flasks were allowed to stand overnight at room temperature to equilibrate the pyrene and micelles. For fluorescence spectra, the excitation wavelength (λ_{ex}) was 339 nm. For the excitation spectra, the emission wavelength (λ_{em}) was 390 nm.

(2) Determination of critical micelle temperature (CMT). The fluorescence emission spectra of NR in a 0.2 wt% aqueous $PNiPAAm_{20}$-ONB-$PMCL_{49}$ polymer solution at various temperatures were recorded. At each temperature, the solution was equilibrated for 10 min. The maximum fluorescence intensities were plotted against temperatures for the determination of CMT. For fluorescence spectra, λ_{ex} was 550 nm. For the excitation spectra, λ_{em} was 556 nm.

Preparation of polymeric micelles

Polymeric micelles of PNiPAAm-ONB-PXCL polymers were prepared using a dialysis. Briefly, a solution of PNiPAAm-ONB-PXCL polymer (30 mg) in DMF (5 mL) was placed in a dialysis bag with a molecular weight cutoff (MWCO) of 3500 Da and dialyzed against deionized water at an ambient temperature for 24 h. The water was replaced at 2 h intervals.

Dynamic light -scattering

Micelles size and distribution were investigated using DLS (Zetasizer Nano ZS, Malvern, UK) with an argon laser operating at 632.8 nm and a fixed scattering angle of 90^{o} at 20 ℃. Measurements were recorded after the filtering of an aqueous

micellar solution (C = 0.3 g L^{-1}) by using a microfilter with an average pore size of 0.2 μm (Advantec MFS, Inc., Dublin, CA, USA). The average size distribution of the aqueous micellar solution was determined using the CONTIN program developed by Provencher and Hendrix [38].

Transmission electron microscopy

Microscopic images of the micelles were observed using a transmission electron microscope (JEM 1200-EXII, Tokyo, Japan). Drops of micelle solution (0.3 g L^{-1}, not containing a staining agent) were placed on a carbon film- coated copper grid and dried at room temperature. Micelles were observed at an accelerating voltage of 100 kV.

Determination of drug -loading content and drug entrapment efficiency

$PNiPAAm_{20}$-ONB-$PMCL_{49}$ (50-fold CMC value) was dissolved in 6 mL of methylene chloride by using oil-in-water evaporation. The anti-inflammatory drug indomethacin (IMC) was added to the polymer in a 1:1 weight ratio to serve as a model drug. The solution was added dropwise to 150 mL of distilled water. Sonication was applied for 1 h at an ambient temperature to reduce the droplet size. The emulsion was stirred at an ambient temperature overnight to evaporate the methylene chloride. The unloaded IMC residue was removed by filtering through a Teflon filter (Whatman) with an average pore size of 0.45 μm, and the micelles were obtained by vacuum drying. A weighed amount of micelles was then disrupted by adding a 10-fold excess volume of DMF. Drug content was assayed spectrophotometrically at 320 nm using a diode array UV-Vis spectrophotometer. The following equations were used to calculate the drug-loading content and drug entrapment efficiency:

Drug-loading content (%)

= (weight of drug in the micelles / weight of micelles) × 100 (1)

Drug entrapment efficiency (%)

= (weight of drug in the micelles / weight of drug provided initially) × 100 (2)

Analysis of in vitro drug release

Appropriate amounts of IMC-loaded micelles (110.2 mg) were weighed and suspended in 10 mL of PBS (0.1 M, pH 7.4 or 5.0). The micellar solution was introduced to a dialysis membrane bag (MWCO = 3500 Da), and the bag was placed in 50 mL of a PBS release medium. The medium was shaken (30 revolutions/min) or exposed to UV light at 42 ℃. At predetermined intervals, 3 -mL aliquots of the aqueous solution were withdrawn from the release medium, and an identical volume of fresh buffer solution was added. The concentration of released IMC was determined using a UV-Vis spectrophotometer at a wavelength of 320 nm. The rate of controlled drug release was measured according to the cumulatively released weight of IMC by using the calibration curve for IMC.

Cell culture

HeLa cells were maintained in DMEM/F12 1:1 medium containing 10% FBS and 1% antibiotic-antimycotic at 37 ℃ in a humidified atmosphere with 5% carbon dioxide (CO_2).

Flow cytometric analysis of the uptake of doxorubicin-loaded micelles

HeLa cells were seeded in 35 -mm dishes (1.5×10^5 cells/dish) and cultured overnight. DOX-loaded $PNiPAAm_{20}$-ONB-$PMCL_{49}$ micelles and free DOX (447 ng mL^{-1}) dissolved in DMEM/F12 1:1 medium with 1% FBS, were then added and incubated for 5 and 30 min. Cells were trypsinized and fixed with 4% paraformaldehyde for 15 min prior to analysis. A BD FACS-Calibur flow cytometer, equipped with a 488 -nm argon laser, and CellQuest software were used for analysis. An FL2 channel captured the fluorescence of DOX. Each experiment was conducted in triplicate.

Microscopic evaluation of the intracellular distribution of doxorubicin and

doxorubicin-loaded micelles

HeLa cells were seeded in 35 -mm dishes (1×10^5 cells/dish), and cultured overnight. DOX-loaded $PNiPAAm_{20}$-ONB-$PMCL_{49}$ micelles and free DOX (447 ng mL^{-1}) dissolved in DMEM/F12 1:1 medium with 1% FBS, were then added and incubated for 5 min, 30 min, and 2 h. Cells were fixed with 4% paraformaldehyde and nuclei -stained with 1 μg $mL^{-1}$of Hoechst 33342. Images were visualized using an Olympus IX71 fluorescence microscope (Japan).

Determination in vitro cellular viability

The cytotoxicity of free DOX, blank micelles and DOX-loaded micelles were investigated using MTS assay with a Promega CellTiter 96® AQueuous One Solution kit. The assay was performed according to the manufacturer's instructions with minor modifications. Briefly, HeLa cells were seeded in a 24-well plate (3×10^4 cells/well) overnight, and then treated with various concentrations of free DOX, polymers and freeze-dried DOX-loaded micelles or a DMSO vehicles added to DMEM/F12 1:1 medium with 1% FBS in a humidified 37 ℃ incubator supplied with 5% CO_2. After 48 h, the medium in each well was removed and replaced with 350 μL of warm PBS and 35 μL of CellTiter 96® AQueuous One Solution. The mixture was then incubated at 37 ℃ for 4 h. After incubation, 110 μL of supernatant from each well was moved to a 96-well plate and absorbance was measured at 485 nm by using an ELISA reader (Hidex, Finland).

Results and discussion

Synthesis and characterization of PNiPAAm-ONB-PXCL block copolymer

Scheme 1 shows the strategy for synthesizing the temperature-responsive and photo-cleavable PNiPAAm-ONB-PXCL copolymer. We selected the difunctional initiator 5-hydroxy-2-nitrobenzyl alcohol, which contains two hydroxyl groups of benzyl and phenol, as the photo-responsive molecule because of its chemical stability

and rapid cleavage in response to near-UV irradiation (wavelength ＞ 320 nm) [39]. First, the benzyl hydroxyl group initiated the ROP of ε-CL or 4-substituted-ε-caprolactone (MCL and BCL) catalyzed by $SnOct_2$. Nucleophilic substitution etherified the phenolic hydroxyl group of the resulting HONB-PXCL with PNiPAAm-OTs in DMF at 60 ℃ to provide the PNiPAAm-ONB-PXCL polymer. Table 1 lists our coupling results. The isolated yields were moderate to high. The theoretical number-average molecular weight ($M_{n,th}$) and number-average molecular weight determined by GPC ($M_{n,GPC}$) showed good agreement. FT-IR and ^{1}H NMR results confirmed the effective coupling of PNiPAAm to provide PNiPAAm-ONB-PXCL. The representative ^{1}H NMR spectrum (Fig. 1B) revealed the presence of signals from PNiPAAm. The resonance peaks could be assigned to the corresponding hydrogen atoms of the PNiPAAm blocks at δ = 5.92-6.68 (H_q, -N*H*), 4.01 (H_o, -C*H*(CH_3)$_2$), 2.02-2.58 (H_n, H_m, -C*H*- and -CH_2-), and 1.19 (H_p, -CH(CH_3)$_2$). The resonance peaks of the PMCL blocks are shown at δ = 4.10 (H_i, -CH_2O-), 2.30 (H_e, -CH_2-), 1.40-1.80 (H_{f+g+h}, -C*H*-, and -CH_2-), and 0.95 (H_j, -CH_3). The IR spectrum of PNiPAAm-ONB-PXCL (Fig. 2C) indicated typical carbonyl absorptions of an ester of ONB-PXCL, and an amide of PNiPAAm at 1720 cm^{-1}, and 1650 cm^{-1}, respectively. Fig. 3 shows the representative GPC curves of $PNiPAAm_{20}$-ONB-$PMCL_{49}$ compared with those of the original HONB-$PMCL_{49}$. The GPC traces of $PNiPAAm_{20}$-ONB-$PMCL_{49}$ with a shift in the peak towards the higher molecular weight region, compared with the peak of the original HONB-$PMCL_{49}$. The GPC chromatogram of $PNiPAAm_{20}$-ONB-$PMCL_{49}$ showed a shoulder in low molecular weight side, which may be attributed to the presence of trace of HONB-PXCL in the reaction product.

Table 1 shows the thermal behaviors of the block copolymers PNiPAAm-ONB-PXCL. The PNiPAAm-ONB-PXCL copolymers exhibited amorphous T_g. DSC indicated that,

fixing the length of the PCL block (PCL_{12}: M_n = 1370 g mol^{-1}) and increasing the length of the PNiPAAm block increased T_gs. If we fixed the M_n of the PNiPAAm at 1210 g mol^{-1} ($PNiPAAm_{10}$), T_g decreased from 52.6 ℃ to -56.3 ℃ when the length of the PMCL block increased from $PMCL_{13}$ to $PMCL_{49}$ because the flexibility of the PMCL block increased when larger amounts of MCL were incorporated into the macromolecular backbone.

Degradation of photolabile PNiPAAm-ONB-PXCL block copolymers

We investigated the photolytic degradation of the polymer by UV-Vis spectroscopy, observing the spectra changes of a polymer solution over irradiation time. For this purpose, we dissolved 2 mg $PNiPAAm_{20}$-ONB-$PMCL_{47}$ in 1 mL inhibitor-free THF and irradiated the solution with UV lamp (352 nm, 8 × 8 W) for a given amount of time. The experiment was carried out at ambient temperature. The intensity of the band located at 308 nm, associated to the nitro-aromatic moiety, decreases with the irradiation time (Fig. 4A). To further prove the cleavage of the copolymer, the products obtained after irradiation were analyzed by GPC. Fig. 4B shows the GPC traces of the $PNiPAAm_{20}$-ONB-$PMCL_{47}$ copolymer before and after photoirradiation. After irradiation, the peak shift to a lower molecular weight region, corresponding to the dissociated PXCL and PNiPAAm blocks. Additionally, the photodegradation was followed by ^1H NMR. Fig. 4C, significant changes in chemical shifts are observed. Upon degradation, the ester linkage between ONB and PXCL is converted to an aldehyde functionality (at approximately 9.8 ppm), indicating that photolysis took place.

Lower critical solution temperature behaviours

PNiPAAm is a temperature-sensitive polymer that undergoes a coil-to-globule transition upon heating. This transition results in the precipitation of PNiPAAm or related copolymers. We characterized the LCST behaviours of the

PNiPAAm-ONB-PXCL copolymer solutions by measuring their cloud points (CP). As shown in Fig. 5A, the optical properties of the PNiPAAm-ONB-PXCL copolymers (transmittance at 500 nm) change upon heating. We determined the LCST at the temperature at which optical transmittance was 50%. Table 1 lists our LCST results. When a hydrophilic block is included, the LCSTs of the corresponding BCPs increase. However, when a hydrophobic block is incorporated, the LCSTs decrease.[40] At the fixed length of the hydrophobic block (PCL_{12}), the LCST values of the copolymers PNiPAAm-ONB-PCL decreased from 45.8 ℃ to 32.5 ℃ when the length of PNiPAAm segment increase from $PNiPAAm_{10}$ to $PNiPAAm_{50}$, due to the hydrophilicity of PNiPAAm segment reduced. However, as the hydrophilic block was fixed at $PNiPAAm_{10}$, the LCST values of the copolymers $PNiPAAm_{10}$-ONB-PMCL increased from 39.5 ℃ to 51.1 ℃ when the length of PMCL segment increase from $PMCL_{13}$ to $PMCL_{49}$, which can be attributed to the side substituent groups reduce the hydrophobicity of the PMCL. Additionally, when using the longer and more bucky the PBCL block, the transition was very weak, even be lost. No transition behaviour in $PNiPAAm_{10}$-ONB-$PBCL_{55}$ was observed. The $PNiPAAm_{10}$-ONB-$PBCL_{55}$ aqueous solution remained transparent with nearly no decrease in transmittance, suggesting that the larger-sized aggregates of $PNiPAAm_{10}$-ONB-$PBCL_{55}$ had not formed. These observations indicated that the hydrophilicity of the PNiPAAm block and the chain length or the substitute group of the PXCL block significantly influence the transition temperature of the corresponding copolymer. It was found that the LCST of $PNiPAAm_{20}$-ONB-$PMCL_{49}$ is close to the temperature of cancer cell (39.3 ℃).

Fig. 5B shows the optical transmittances of a 0.2 wt% aqueous solution of $PNiPAAm_{20}$-ONB-$PMCL_{49}$ at a wavelength of 550 nm as a function of temperature in heating and cooling processes. The CP of $PNiPAAm_{20}$-ONB-$PMCL_{49}$ in water was 39.3 ℃ during the heating process and 38.4 ℃ during the cooling process. We

observed minimal hysteresis between heating and cooling. The thermo-induced LCST transition of $PNiPAAm_{20}$-ONB-$PMCL_{49}$ was reversible.

Micelles of PNiPAAm-ONB-PXCL

The amphiphilic nature of PNiPAAm-ONB-PXCL polymers, which consist of a hydrophilic PNiPAAm and a hydrophobic ONB-PXCL segment, enables micelles to form in water. In this study, we investigated the characteristics of the PNiPAAm-ONB-PXCL micelles in aqueous phase by using fluorescence techniques. We determined the CMC of PNiPAAm-ONB-PXCL in aqueous phase by using pyrene as a probe molecule. We observed that the fluorescence intensity of the excitation spectrum of pyrene (data not shown) increased with increasing PNiPAAm-ONB-PXCL polymer concentration. We used the characteristic feature of the pyrene excitation spectrum, a red-shift of the (0,0) band from 331 to 334 nm or from 334 to 336 nm during partitioning into a micellar hydrophobic core, to determine the CMC values of PNiPAAm-ONB-PXCL polymers. Fig. 6 shows the intensity ratios I_{III}/I_I (I_{334}/I_{331}or I_{336}/I_{334}) of pyrene excitation spectra versus the logarithm of PNiPAAm-ONB-PXCL polymers concentrations. We determined CMC based on the interaction of straight line segments drawn through the points of the lowest polymer concentrations, which lie on a nearly horizontal line, and the points of the rapidly rising region of the plot. Table 2 lists the CMC values of the various PNiPAAm-ONB-PXCL polymers. The PNiPAAm-ONB-PXCL polymers formed micelles in the aqueous phase, and the CMCs ranged from 1.4 to 185.6 mg L^{-1}. The PNiPAAm-ONB-PXCL polymers exhibited lower CMC values than those of the surfactant (e.g. 2.3 g L^{-1} for sodium dodecyl sulfate in water), indicating thermodynamically favorable self-association in PNiPAAm-ONB-PXCL. Polymeric micelles with lower CMC values are usually more stable in drug delivery applications, because they remain stable in a dilute form in the blood after being administrated.[41]

As the hydrophilicity of the hydrophilic segment or the hydrphobicity of the hydrophobic segment increased, reduced CMC values were observed. At the fixed length of the hydrophilic block ($PNiPAAm_{10}$), the CMC values of the copolymers PNiPAAm-ONB-PMCL reduced from 111.4 to 5.8 mg L^{-1} when the hydrophobic PMCL chain length increase from $PMCL_{13}$ to $PMCL_{49}$, and the hydrophobic segment changed from $PMCL_{49}$ to $PBCL_{55}$, the CMC values decreased from 5.8 to 1.4 mg L^{-1}, which can be attributed to that the PBCL is more hydrophobic than the PMCL, making the association of copolymer molecules occur at a lower concentration. As the length of the hydrophilic (PNiPAAm) segment increased from $PNiPAAm_{10}$ to $PNiPAAm_{50}$, an increased CMC values also exhibited.

We further investigated the thermo-induced formation of micelle of $PNiPAAm_{20}$-ONB-$PMCL_{49}$ in water by using fluorescence spectroscopy. We used NR as the hydrophobic fluorescence probe because its fluorescence is negligible in water but increases substantially in a hydrophobic environment such as in the core of micelles. In addition, its wavelength of maximal absorption (λ_{max}) at 553 nm is far from the interfering absorptions of the block copolymers. Fig. 7A shows the fluorescence emission spectra of NR in a 0.2 wt% aqueous solution of $PNiPAAm_{20}$-ONB-$PMCL_{49}$ at various temperatures during the heating process. When the temperature was ＞ 30 ℃, the fluorescence emission intensity increased substantially, indicating the association of the molecularly dissolved polymer chains with micelles and the sequestering of dye molecules into the core. The CMT, determined from the plot of maximum fluorescence intensity versus temperature, was 33.9 ℃ (Fig. 7B).

The mean hydrodynamic diameters of micelles incorporating IMC and blank micelles, ranged from 130.5 to 172.7 nm and from 117.3 to 129.6 nm, respectively. The micelles incorporating IMC were larger than the blank micelles because of the

incorporation of the hydrophobic drug; however, micelle size remained < 200 nm for all formations. A small particle size (< 200 nm) can reduce the level of uptake in the reticulate endothelial system, minimize renal excretion, and increase the accumulation of micelle-encapsulated drugs in tumors though increased permeability and retention [42]. Because the polymer concentration was 50 times the CMC value, the mean diameter of the micelles increased with increasing the length of the hydrophilic segment. The micelle sizes of the $PNiPAAm_{20}$ series polymers were larger than those of the $PNiPAAm_{10}$ series polymers with similar length hydrophobic segments, which could be attributed to increase hydrated diameter caused by the longer length of the hydrophilic PNiPAAm block. However, at a fixed hydrophilic block length ($PNiPAAm_{10}$), micelles size decreased with increasing length of the hydrophobic segment (PMCL). These responses indicated that micelle size is dependent on the polymer composition (i.e., the length of the hydrophobic segment or the hydrophilicity of the hydrophilic moiety in the chain). The PNiPAAm-ONB-PXCL micelles were associated with reasonable narrow distribution, with a PDI < 0.33. Fig. 7C shows hydrodynamic size as a function of temperature for a 0.2 wt% aqueous micelle solution of $PNiPAAm_{20}$-ONB-$PMCL_{49}$. When the temperature increase from 25 to 60 ℃, micelle size increased from 81 to 95 nm. However, when the temperature decrease from 60 to 25 ℃, micelle size decreased from 102 to 78 nm. We consider this phenomenon to result from decreased micellar hydration at higher temperatures, leading to minor aggregation.

Fig. 8 shows the spherical morphology of $PNiPAAm_{20}$-ONB-$PMCL_{49}$ micelles. When the drug was incorporated, micelle size marginally increased (Fig. 8B). The diameters measured using DLS were similar to those estimated using the TEM images.

Photo-cleavable behaviours of micelles

We evaluated micelles photodegradation at various irradiation times by monitoring

changes in NR fluorescence [43]. We recorded the reduction in NR fluorescence intensity at 556 nm. After dissolving NR and $PNiPAAm_{20}$-ONB-$PMCL_{49}$ in THF (0.5 mg mL^{-1}, NR to polymer ratio: 1:3), water was added to induce micelle formation and concomitant NR encapsulation by the micelle core. We then removed THF by evaporation and filtered the nonsolubilized NR by using microfiltration (0.2 -μm pore filter). We adjusted the final micelle concentration to 0.2 mg mL^{-1}. Fig. 9A shows the fluorescence emission spectra of NR loaded in the $PNiPAAm_{20}$-ONB-$PMCL_{49}$ micelle before and after short-duration UV irradiation ($<$ 1h). Fig. 9B shows normalized fluorescence plotted against time, with and without UV irradiation of the solution. Emission intensity remained constant over time in the absence of irradiation, indicating the stable encapsulation of the dye in a hydrophobic environment. By contrast, the emission intensity reduced by $<$ 47% after only 10 seconds of irradiation. The micelles exhibited photolabile properties in response to light activation. We used TEM to observe the morphologicaly changes after UV irradiation. Figs. 8A and 8C show the images collected before and after UV irradiation (60 s). The TEM micrographs showed distinct morphologies, confirming the rapid disintegration of the NR-loaded micelles in the aqueous solution. Prior to irradiation, micelles size was uniform. However, after exposure to UV light, we observed broken micelles, indicating that a short duration of irradiation induced changes assembly state. The observed rate of fluorescence quenching was rapid, indicating a burst release of loaded NR into the aqueous medium.

Evaluation of drug -loading content and entrapment efficiency

We determined the drug-loading content and drug entrapment efficiency of the polymeric micelles by using UV-Vis absorption spectroscopy. We selected IMC, a common, hydrophobic, non-steroidal, anti-inflammatory drug as a model drug to investigate drug-loading in the hydrophobic core. The maximum absorption peak of

IMC was proportional to its concentration at 320 nm. After releasing IMC and removing the polymer precipitate, we determined the amount of loaded IMC from the absorbance at 320 nm. Table 2 lists the calculated drug-loading content and entrapment efficiency values. At a constant feed weight ratio (1:1), the drug-loading content and entrapment efficiency was 14.1% and 28.2%, respectively. Drug-loading content and entrapment efficiency increased with increasing hydrophilicity of the hydrophilic segment, or increasing hydrphobicity of the hydrophobic segment.

Stimuli -responsive release of indomethacin

We evaluated the time-dependent release of IMC in various conditions by using dialysis. Fig. 10 shows the release profiles of IMC from the IMC micelles of $PNiPAAm_{20}$-ONB-$PMCL_{49}$. Environmental factors, such as temperature, and light, significantly affected the release of IMC from micelles. The IMC release rate increased when the temperature increased from 25 to 42 ℃. We observed that increasing the temperature increased the rate of diffusion, to accelerate drug release. When we increased the temperature higher than the LCST (39.3 ℃), the hydrophilicity of the PNiPAAm segments decreased. Temperatures ＞39.3 ℃ disturbed the hydrophilic-hydrophobic balance of micelles, causing their disassembly, and release of the loaded drugs. Compared with the released rated in the absence of UV irradiation, the release rate of IMC was considerably more rapid under UV irradiation at 42 ℃, with approximately ~ 90% of the encapsulate IMC released in a sustained manner during the first 7 h. These results confirmed our hypothesis that burst release is achieved by the rapid disintegration of the $PNiPAAm_{20}$-ONB-$PMCL_{49}$ micelle core. Tang et al. reported light-triggered burst release from polymer nanoparticles, prepared by emulsification, using self-immolative monomers [43]. The concept of self-immolative polymers could be applied to prepared BCP micelles, in which core degradation can be activated by removing a small number of trigger units.

Cellular uptake profile of doxorubicin-loaded micelles

Amphiphilic polymers can transport drugs through the formation of micelles. Polymer micelles carrying numerous anti-cancer chemotherapies are currently undergoing clinical trials [44]. In this study, we investigated the drug-carrying abilities of $PNiPAAm_{20}$-ONB-$PMCL_{49}$ polymeric micelles by using DOX, a potent anti-tumor drug. The self-fluorescent nature of this drug facilitated the identifying and quantifying of the entry of drug-loaded micelles into cells [45-46].

We prepared DOX-loaded $PNiPAAm_{20}$-ONB-$PMCL_{49}$ micelles by using dialysis, recording the uptake of micelles and free DOX of equal concentration (458.2 ng mL^{-1}) at 5 and 30 min by using flow cytometry (Fig. 11A). One feature of $PNiPAAm_{20}$-ONB-$PMCL_{49}$ encapsulated DOX is the relatively fast entry and accumulation into cells, compared with its free-form counterpart. The geometric mean fluorescence intensity in HeLa cells treated with DOX-loaded $PNiPAAm_{20}$-ONB-$PMCL_{49}$ was approximately 5.5-fold higher (64.7 vs. 11.8) than in HeLa cells treated with free DOX (Fig. 11B). We observed similar trends in the 30 -min treatment group (111.8 vs. 20.6). Substantially greater uptake of $PNiPAAm_{20}$-ONB-$PMCL_{49}$-encapsulated DOX than free DOX suggested that the formation of drug-loaded micelles facilitates drug entry into target cells, which could be associated with the differing underlying entry mechanisms of encapsulated DOX and free DOX [46].

We conducted various fluorescence microscopic experiments to determine the intracellular distributions of DOX-loaded $PNiPAAm_{20}$-ONB-$PMCL_{49}$ micelles or free DOX after entry. Fig. 12 shows our results, from left to right, of DOX fluorescence, nuclear- stained Hoechst 33342, and an overlay of the images. These images revealed that free DOX and $PNiPAAm_{20}$-ONB-$PMCL_{49}$-encapsulated DOX had distinct temporal and spatial entry patterns. Free DOX accumulated in cells at a substantially

slower rate than PNiPAAm$_{20}$-ONB-PMCL$_{49}$-encapsulated DOX did, with minimal fluorescence after 5 and 30 min of treatment, and visible fluorescence after 2 h of treatment (Figs. 12A and 12C). DOX fluorescence predominantly concentrated in cell nuclei, which could be an inherent tendency of free DOX [47]. By contrast, in HeLa cells treated with DOX-loaded PNiPAAm$_{20}$-ONB-PMCL$_{49}$ for 5, 30 min, or 2 h, DOX fluorescence was concentrated in the cytosol (Figs. 12D and 12F). These differences could be attributed to free DOX entering cells through passive diffusion, whereas PNiPAAm$_{20}$-ONB-PMCL$_{49}$ micelle-encapsulated DOX penetrates the plasma membrane through endocytosis [46, 48]. Another possible reason for the trend is that endocyted DOX-loaded micelles are trapped in acidic endocytic compartments and gradually release their DOX cargo in a low pH environment. Because this process is relatively slow, micelle-transported DOX is unable to reach the nuclei as fast as free DOX does [49]. We observed more intense nuclear fluorescence in HeLa cells treated with DOX-loaded PNiPAAm$_{20}$-ONB-PMCL$_{49}$ for 2 h compared with in those treated for 5 min (Figs. 12F and 12D). Entry of nuclei by DOX confirms that PNiPAAm$_{20}$-ONB-PMCL$_{49}$ micelle-encapsulated DOX has been released and reached its pharmacological target. Overall, our data demonstrate that PNiPAAm$_{20}$-ONB-PMCL$_{49}$ micelle facilitates the uptake of encapsulated cargo, and are thus potentially useful as transporters of bioactive molecules into cells.

In vitro cytotoxicities of the polymer and doxorubicin-loaded micelles

We evaluated the in vitro cytotoxicities of the PNiPAAm$_{20}$-ONB-PMCL$_{49}$ polymer, DOX-loaded micelles and free DOX by using MTS assay in HeLa cells with various polymer concentrations or DOX dosages. To eliminate any unwanted cytotoxic effects of PNiPAAm$_{20}$-ONB-PMCL$_{49}$, we assessed the viability of cells loaded with increasing amounts of PNiPAAm$_{20}$-ONB-PMCL$_{49}$ by using a Promega CellTiter 96® AQueuous One Solution kit. We incubated the HeLa cells with various concentrations

of $PNiPAAm_{20}$-ONB-$PMCL_{49}$ for 48 h before reacting with the MTS reagent, which is bioreduced by esterase in living cells to formazan, enabling spectrophotometric analysis absorbance at 485 nm. Fig. 13A shows the relative percentages of cells treated with various concentrations of $PNiPAAm_{20}$-ONB-$PMCL_{49}$. Compared with the control, cell viability was $>$ 80% at a polymer concentration ranging from 1 to 1000 μg mL^{-1}. Fig. 13B shows the in vitro cytotoxicities of the DOX-loaded micelles and free DOX at various DOX dosages (0.125 - 10 μg mL^{-1}). DOX-loaded $PNiPAAm_{20}$-ONB-$PMCL_{49}$ micelles effectively inhibited the proliferation of HeLa cells with a half-maximal inhibitory concentration (IC_{50}) of 5 μg mL^{-1}. The DOX-loaded micelles inhibited cancer cell proliferation to a greater extent than free DOX did, which could have been caused by the DOX-loaded micelles rapidly entering cells and releasing of DOX under irradiation.

Conclusions

In this study, we synthesized and characterized thermo-responsive PNiPAAm-ONB-PMCL block copolymers with a photo-cleavable junction between the hydrophilic and hydrophobic blocks by using ^1H NMR, FT-IR, GPC, and DSC. The thermo-induced LCST transition of $PNiPAAm_{20}$-ONB-$PMCL_{49}$ was reversible. The copolymers formed micelles in aqueous solution, had hydrodynamic sizes $<$ 200 nm, and were spherical. Light triggered the burat of particles and release of encapsulated drug. We evaluated HeLa cell viability in response to these particles at concentrations $<$ 1000 μg mL^{-1}, and observed low toxicity to HeLa cells. $PNiPAAm_{20}$-ONB-$PMCL_{49}$-encapsulated DOX enters and accumulates into cells at a substantially faster rate than its free- form counterpart does. Therefore, our study results indicate that thermo- and light- sensitive $PNiPAAm_{20}$-ONB-$PMCL_{49}$ block copolymers can be of used in targeted drug delivery.

Acknowledgements

The research was supported by grants from National Science Council (NSC 102-2221-E-182-068) and Chang Gung Memorial Hospital (CMRPD5D0011).

References

1 J. M. Schumers, C. A. Fustin, and J. F. Gohy, *Macromol. Rapid Commun.* 2010, **31**, 1588-1607.

2 J. Babin, M. Pelletier, M. Lepage, J. F. Allard, D. Morris, and Y. Zhao, *Angew. Chem. Int. Ed.* 2009, **48**, 3329-3332.

3 F. D. Jochum, and P. Theato, *Chem. Commun.* 2010, **46**, 6717-6719.

4 D. Han, X. Tong, and Y, Zhao, *Macromolecules* 2011, **44**, 437-439.

5 S. M. Lee, and S. B. T. Nguyen, *Macromolecules* 2013, **46**, 9169-9180.

6 T. Krasia-Christoforou, and T. K. Georgiou, *J. Mater. Chem. B* 2013, **1**, 3002-3025.

7 S. Wong , M. S. Shim, and Y. J. Kwon, *J. Mater. Chem. B* 2014, **2**, 595-615.

8 J. Rao, Z. Luo, Z. Ge, and H. Liu, *Biomacromolecules* 2007, **8**, 3871-3878.

9 C. Engler, D. K. Bonner, H. G. Bus, E. Y. Cheung, and P. T. Hammond, *Soft Matter.* 2011, **7**, 5627-5637.

10 M. S. Shim, and Y. J. Kwon, *Biomaterials* 2010, **31**, 3404-3413.

11 J. Huang, C. L. Hastings, G. P. Duffy, H. M. Kelly, J. Raeburn, D. J. Adams, and A. Heise, *Biomacromolecules* 2013, **14**, 200-206.

12 Y. Cheng, C. He, C. Xiao, J. Ding, X. Zhuang, Y. Huang, and X. Chen, *Biomacromolecules* 2012, **13**, 2053-2059.

13 S. Kumar, J. F. Allard, D. Morris, Y. L. Dory, M. Lepage, and Y. Zhao, *J. Mater. Chem.* 2012, **22**, 7252-7257.

14 G. Liu, and C. M. Dong, *Biomacromolecules* 2012, **13**, 1573-1583.

15 F. Meng, W. F. Hennink, and Z. Zhong, *Biomaterials* 2009, **30**, 2180-2198.

16 A. Sulistio, A. Blencowe, A. Widjaya, X. Zhang, and G. Qiao, *Polym. Chem.* 2012, **3**, 224-234.

17 R. P. Johnson, Y. I. Jeong, J. V. John, C. W. Chung, D. H. Kang, M. Selvaraj, H. Suh, and I. Kim, *Biomacromolecules* 2013, **14**, 1434-1443.

18 X. Jiang, C. A. Lavender, J. W. Woodcock, and B. Zhao, *Macromolecules* 2008, **41**, 2632-2643.

19 L. Ionov, and S. Diez, *J. Am. Chem. Soc.* 2009, **131**, 13315-13319.

20 Y. Wu, H. Hu, J. Hu, T. Liu, G. Zhang, and S. Liu, *Langmuir* 2013, **29**, 3711-3720.

21 E. Blasco, V. K. J. Schmidt Bernhard, C. Barner-Kowollik, M. Piñol, and L. Oriol, *Polym. Chem.* 2013, **4**, 4506-4514.

22 X. Wang, G. Jiang, X. Li, B. Tang, Z. Wei, and C. Mai, *Polym. Chem.* 2013, **4**, 4574-4577.

23 J. Yin, H. Hu, Y. Wu, and S. Liu, *Polym. Chem.* 2011, **2**, 363-371.

24 Z. Feng, L. Lin, Z. Yan, and Y. Yu, *Macromol. Rapid Commun.* 2010, **31**, 640-644.

25 Y. Wu, H. Hu, J. Hu, T. Liu, G. Zhang, and S. Liu, *Langmuir* 2013, **29**, 3711-3720.

26 J. M. Schumers, J. F. Gohy, and C. A. Fustin, *Polym. Chem.* 2010, **1**, 161-163.

27 J. S. Katz, S. Zhong, B. G. Ricart, D. J. Pochan, D. A. Hammer, and J. A. Burdick, *J. Am. Chem. Soc.* 2010, **132**, 3654-3655.

28 B. Yan, J. C. Boyer, N. R. Branda, and Y. Zhao, *J. Am. Chem. Soc.* 2011, **133**, 19714-19717.

29 E. Cabane, V. Malinova, and W. Meier, Macromol. Chem. Phys. 2010, **211**, 1847-1856.

30 E. Cabane, V. Malinova, S. Menon, C. G. Palivan, and W. Meier, *Soft Matter.* 2011, **7**, 9167-9176.

31 H. Zhao, E. S. Sterner, E. B. Coughlin, and P. Theato. *Macromolecules* 2012, **45,** 1723-1736.

32 R. S. Lee, and W. H. Chen, *React. Funct. Polym.* 2011, **71**, 455-462.

33 K. Y. Peng, S. W. Wang, and R. S. Lee, *J. Polym. Sci. Part A: Polym. Chem.* 2013, **51**, 2769-2781.

34 M. Kang, and B. Moon, *Macromolecules* 2009, **42**, 455-458.

35 H. Cai, G. Jiang, Z. Shen, and X. Fan, *Macromolecules* 2012, **45**, 6176-6184.

36 P. Vangeyte, and R. Jérôme, *J. Polym. Sci. Part A: Polym. Chem.* 2004, **42**, 1132-1142

37 H. Kuang, S. Wu, Z. Xie, F. Meng, X. Jing, and Y. Huang, *Biomacromolecules* 2012, **13**, 3004-3012.

38 S. W. Provencher, and J. Hendrix, *J. Phys. Chem.* 1978, 69, 4237-4276.

39 D. R. Griffin, J. L. Schlosser, S. F. Lam, T. H. Nguyen, H. D. Maynard, A. M. Kasko, *Biomacromolecules* 2013, **14**, 1199-1207.

40 E. S. Gil, S. M. Hudson, *Prog. Polym. Sci.* 2004, **29**, 1173-1222.

41 R. Ranjan, W. J. Brittain, *Macromol. Rapid Commun.* 2007. **28**, 2084-2089.

42 M. Prabaharan, J. J. Grailer, S. Pilla, D. A. Steeber, and S. Q. Gong, *Biomaterials* 2009, **30**, 5757-5766.

43 C. Lv, Z. Wang, P. Wang, and X. Tang, *Langmuir* 2012, 28, 9387-9394.

44 C. Oerlemans, W. Bult, M. Bos, G. Storm, J. F. Nijsen, and W. E. Hennink, *Pharm. Res.* 2010, **27**, 2569-2589.

45 X. Dai, Z. Yue, M. E. Eccleston, J. Swartling, N. K. Slater, and C. F. Kaminski, *Nanomedicine* 2008, **4**, 49-56.

46 Y. Jin, L. Song, y. Su, L. Zhu, Y. Pang, F. Qiu, G. Tong, D. Yan, B. Zhu, and X. Zhu, *Biomacromolecules* 2011, **12**, 3460-3468.

47 M. Sui, W. Liu, and Y. Shen, *J. Control Rel.* 2011, **155**, 227-236.

48 J. Yan, Z. Ye, M. Chen, Z. Liu, Y. Xiao, Y. Zhang, Y. Zhou, W. Tan, and M. Lang, *Biomacromolecules* 2011, **12**, 2562-2572.

49 H. Hillarireau, and P. Couvreur, *Cell Mol Life Sci.* 2009, **66**, 2873-2896.

Figure captions

Fig. 1 Representative ^{1}H NMR spectroscopy of (A) HONB-$PMCL_{49}$, and (B) $PNiPAAm_{20}$-ONB-$PMCL_{49}$ in $CDCl_3$

Fig. 2 IR spectra of (A) HONB-$PMCL_{49}$, (B) $PNiPAAm_{20}$-OTs, and (C) $PNiPAAm_{20}$-ONB-$PMCL_{49}$

Fig. 3 GPC curves of (A) HONB-$PMCL_{49}$, and (B) $PNiPAAm_{20}$-ONB-$PMCL_{49}$

Fig. 4 (A) Time dependent UV-Vis spectra changes of $PNiPAAm_{20}$-ONB-$PMCL_{47}$ in THF (2 mg ml^{-1}), (B) GPC traces of $PNiPAAm_{20}$-ONB-$PMCL_{47}$ before (I) and after (II) UV light exposure (352 nm, 64 W) for 1 h, (C) ^{1}H NMR of $PNiPAAm_{20}$-ONB-$PMCL_{47}$ after UV irradiation for 1 h in $CDCl_3$

Fig. 5 (A) Phase-transition curves of (●) $PNiPAAm_{10}$-ONB-$PBCL_{55}$, (☆) $PNiPAAm_{10}$-ONB-$PMCL_{49}$, (▲) $PNiPAAm_{10}$-ONB-$PMCL_{39}$, (■) $PNiPAAm_{10}$-ONB-PCL_{12}, (▼) $PNiPAAm_{10}$-ONB-$PMCL_{13}$, (★) $PNiPAAm_{20}$-ONB-$PMCL_{49}$, (◆) $PNiPAAm_{20}$-ONB-PCL_{12}, (○) $PNiPAAm_{50}$-ONB-PCL_{12} in 0.2 wt% in DI water at λ = 500 nm, and (B) Phase-transition curves of $PNiPAAm_{20}$-ONB-$PMCL_{49}$: heating from 25 to 60 ℃ (■), and cooling from 60 to 25 ℃ (▲).

Fig. 6 Plot of I_{III}/I_I intensity ratio (from pyrene excitation spectra; pyrene concentration: (6.1×10^{-7} M) versus the logarithm of concentration (Log C) for (▼) $PNiPAAm_{10}$-ONB-$PMCL_{13}$, (▲) $PNiPAAm_{10}$-ONB-$PMCL_{39}$, (★) $PNiPAAm_{20}$-ONB-$PMCL_{49}$, and (◆) $PNiPAAm_{10}$-ONB-$PMCL_{49}$ (λ_{em} = 390 nm)

Fig. 7 Fluorescence spectra of Nile red (A) in a 0.2 wt% aqueous solution of $PNiPAAm_{20}$-ONB-$PMCL_{49}$ at temperature during the heating process, (B) the plot of maximum fluorescence intensity vs temperature, from which the critical micellization temperature (CMT) was determined, and (C) various of size as a function of solution temperature for $PNiPAAm_{20}$-ONB-$PMCL_{49}$ micelles.

Fig. 8 TEM images of micelles formed by PNiPAAm$_{20}$-ONB-PMCL$_{49}$ (A) blank, (B) with IMC, and (C) UV irradiation for 60 s. Scale bars = 0.2 μm

Fig. 9 (A) Fluorescence spectra of Nile red-loaded PNiPAAm$_{20}$-ONB-PMCL$_{49}$ micelle solution upon light irradiation (352 nm, 8w) for 0, 5, 10, 15, 30, 60 sec and 20, 60 min, and (B) Normalized fluorescence emission intensity vs. time of the NR-loaded micelle solution with and without UV irradiation.

Fig. 10 IMC release from the micelle of PNiPAAm$_{20}$-ONB-PMCL$_{49}$ treated in 0.1 M PBS at different conditions: in pH 7.4 without UV irradiation at 25 ℃ (■) and 42 ℃ (●); at 42 ℃ under UV irradiation in pH 5.0 (▼) and pH 7.4 (▲).

Fig. 11 (A) Flow cytometric histogram profiles of HeLa cells treated with free DOX (A, left), and DOX-loaded PNiPAAm$_{20}$-ONB-PMCL$_{49}$ (A, right) for 5 min and 30 min. Control groups were cells that did not receive any treatment, representing basal fluorescent levels, and (B) Geometric mean fluorescence intensities of free DOX (black) and DOX-loaded PNiPAAm$_{20}$-ONB-PMCL$_{49}$ (gray). Data are mean ± S.E. (n = 3).

Fig. 12 Fluorescent microscopic images of HeLa cells incubated with free DOX for 5 min (A), 30 min (B) and 2 h (C), and with DOX-loaded PNiPAAm$_{20}$-ONB-PMCL$_{49}$ micelles for 5 min (D), 30 min (E) and 2 h (F). For each row, images for left to right show the cells with DOX fluorescence, Hoechst 33342 nuclear staining, and the merged image (scale bar: 50 μm; brightness not proportional to fluorescence intensity).

Fig. 13 The Cell viabilities of HeLa cells treated with (A) various concentrations of PNiPAAm$_{20}$-ONB-PMCL$_{49}$, (B) DOX-loaded PNiPAAm$_{20}$-ONB-PMCL$_{49}$ micelles and free DOX for 48 h, then under UV irradiation 15 sec. Data shown as mean ± S.E. (n = 3)

Scheme 1 Synthesis of the thermo- and photo-responsive PNiPAAm-ONB-PXCL

Table 1 Results of the coupling of HONB-PXCL with TsO-PNiPAAm

Copolymer[a]	Isolated Yield (%)	$M_{n,th}$[b]	$M_{n,GPC}$[c]	M_w/M_n[c]	T_g[d] (℃)	LCST[e] (℃)
$PNiPAAm_{10}$-ONB-PCL_{12}	70	2710	2500	1.10	40.0	45.8
$PNiPAAm_{20}$-ONB-PCL_{12}	55	3840	3470	1.10	64.9	33.5
$PNiPAAm_{50}$-ONB-PCL_{12}	76	7220	6180	1.03	94.4	32.5
$PNiPAAm_{10}$-ONB-$PMCL_{13}$	87	2970	2830	1.15	52.6	39.5
$PNiPAAm_{10}$-ONB-$PMCL_{39}$	65	6340	5000	1.41	-53.3	50.0
$PNiPAAm_{10}$-ONB-$PMCL_{49}$	55	5420	4790	1.51	-56.3	51.1
$PNiPAAm_{10}$-ONB-$PBCL_{55}$	88	7250	6140	1.57	15.0	-
$PNiPAAm_{20}$-ONB-$PMCL_{49}$	56	6550	5340	1.60	-55.2	39.3

[a] Abbreviations: PCL = poly (ε-caprolctone); PMCL = poly (4-methyl-ε-caprolactone); PBCL = poly (4-phenyl-ε-caprolactone); ONB = 5-hydroxy-2-nitrobenzylalcohol; PNiPAAm = poly (*N*-isopropyl acrylic amide).

[b] $M_{n,th} = M_{n,HONB\text{-}PXCL} + M_{n,\ PNiPAAm.}$

[c] Determine by GPC relative to polyethylene glycol standards in $CHCl_3$.

[d] The DSC analysis was conducted from -80 to 250 □ at a heating rate 20 ℃ min^{-1} under nitrogen.

[fe] LCST was determined by spectroscopically at 500 nm in 0.2 wt% aqueous polymer solution. The LCSTs were 41.3, 31.9, and 31.9 ℃ for $PNiPAAm_{10}$, $PNiPAAm_{20}$, and $PNiPAAm_{50}$, respectively.

Table 2 Properties of IMC-loaded PNiPAAm-ONB-PXCL micelles

Copolymer	CMC (mg/L)	Drug entrapment efficiency[a] (%)	Drug loading content[a] (%)	Blank Micelles[b]			Drug Loading Micelle[b]		
				Size (nm)	PDI	Zeta potential (mv)	Size (nm)	PDI	Zeta potential (mv)
$PNiPAAm_{10}$-ONB-PCL_{12}	35.0	6.4	3.2	153.3±20.7	0.21	-26.5			
$PNiPAAm_{20}$-ONB-PCL_{12}	138.0			162.3±60.7	0.18	-30.5			
$PNiPAAm_{50}$-ONB-PCL_{12}	185.6			184.9±14.3	0.13	-36.9			
$PNiPAAm_{10}$-ONB-$PMCL_{13}$	111.4	5.1	2.5	129.6±37.6	0.07	-38.5	130.5±57.9	0.18	-31.0
$PNiPAAm_{10}$-ONB-$PMCL_{39}$	34.2	10.5	5.2	125.2±37.1	0.07	-36.1	168.5±58.3	0.22	-29.9
$PNiPAAm_{10}$-ONB-$PMCL_{49}$	5.8	22.6	11.3	117.3±42.3	0.13	-29.9	172.7±65.0	0.32	-3.5
$PNiPAAm_{10}$-ONB-$PBCL_{55}$	1.4	13.5	6.7	119.2±10.1	0.09	-39.8	135.7±45.6	0.33	-0.8
$PNiPAAm_{20}$-ONB-$PMCL_{49}$	16.9	28.2	14.1	122.9±58.2	0.11	-37.8	164.5±56.9	0.20	-11.2

[a] Feed weight ratio IMC/polymer = 1/1

[b] Determined by DLS

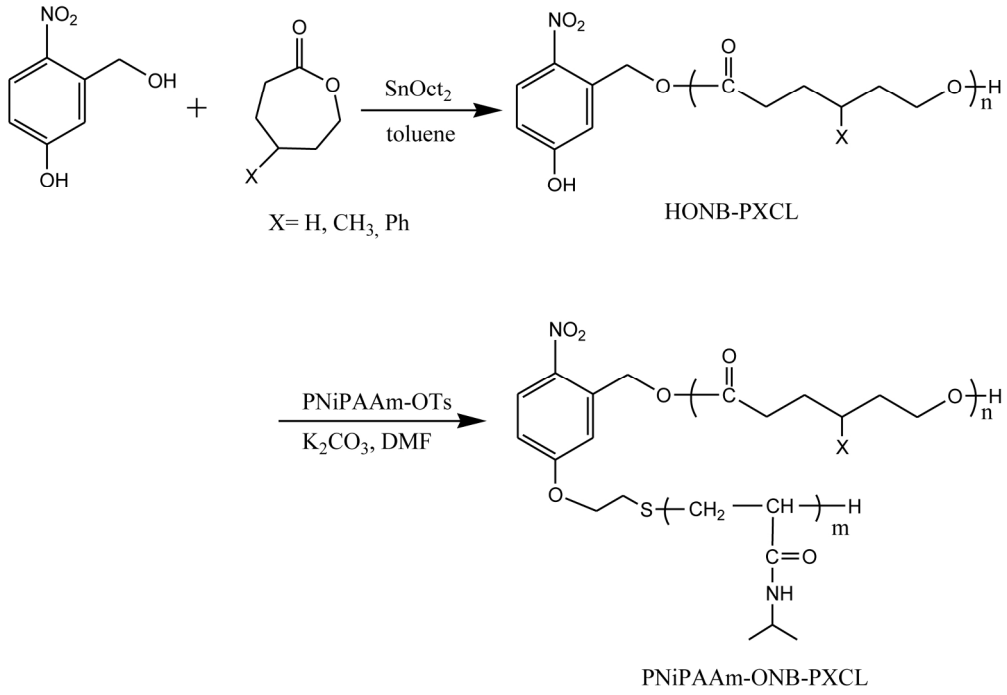

Scheme 1 Synthesis of the thermo- and photo-responsive PNiPAAm-ONB-PXCL

180x137mm (300 x 300 DPI)

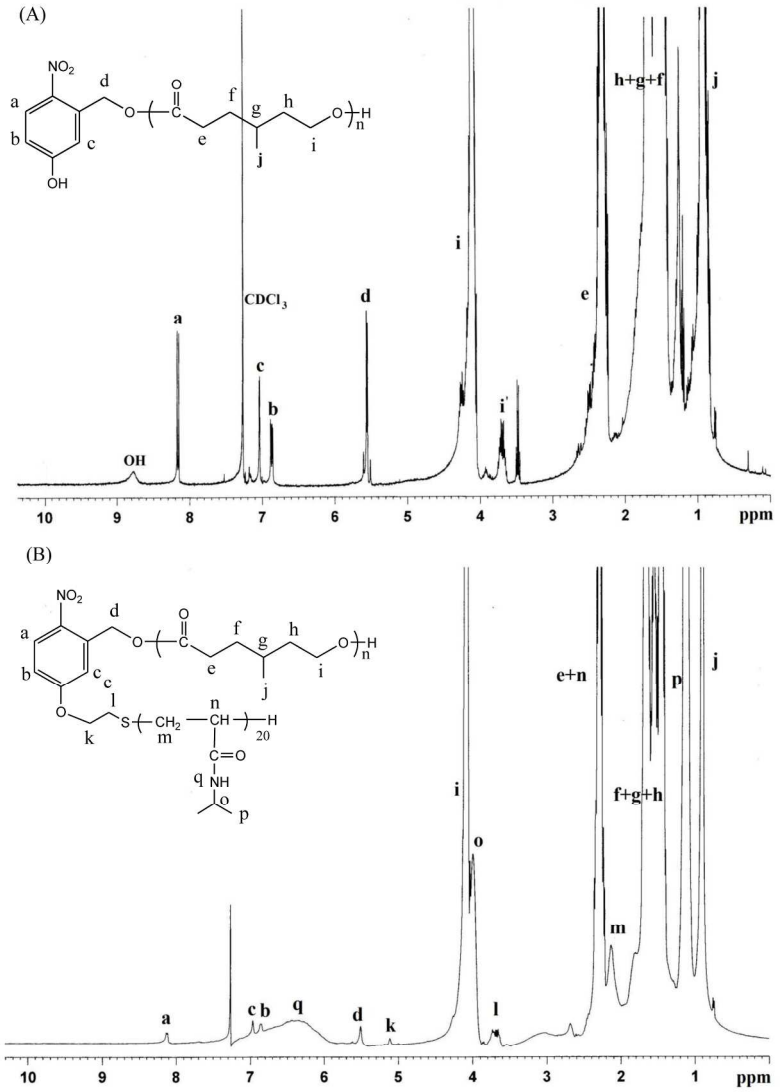

Fig. 1 Representative ^{1}H NMR spectroscopy of (A) HONB-PMCL$_{49}$, and (B) PNiPAAm$_{20}$-ONB-PMCL$_{49}$ in $CDCl_3$

190x259mm (300 x 300 DPI)

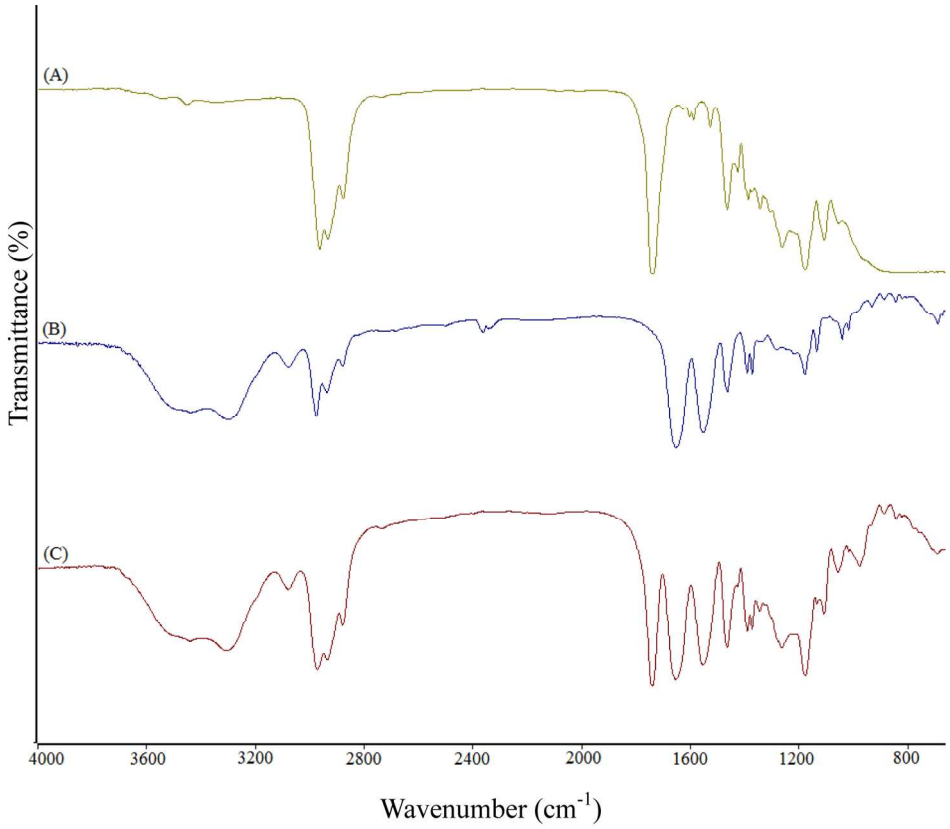

Fig. 2 IR spectra of (A) HONB-PMCL$_{49}$, (B) PNiPAAm$_{20}$-OTs, and (C) PNiPAAm$_{20}$-ONB-PMCL$_{49}$

152x140mm (300 x 300 DPI)

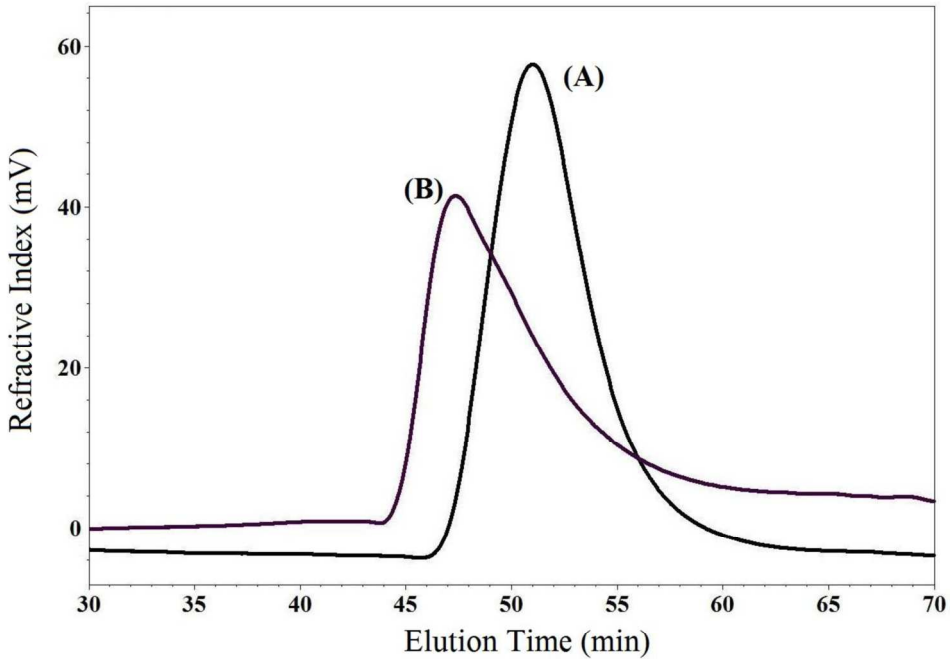

Fig. 3 GPC curves of (A) HONB-PMCL$_{49}$, and (B) PNiPAAm$_{20}$-ONB-PMCL$_{49}$

148x112mm (300 x 300 DPI)

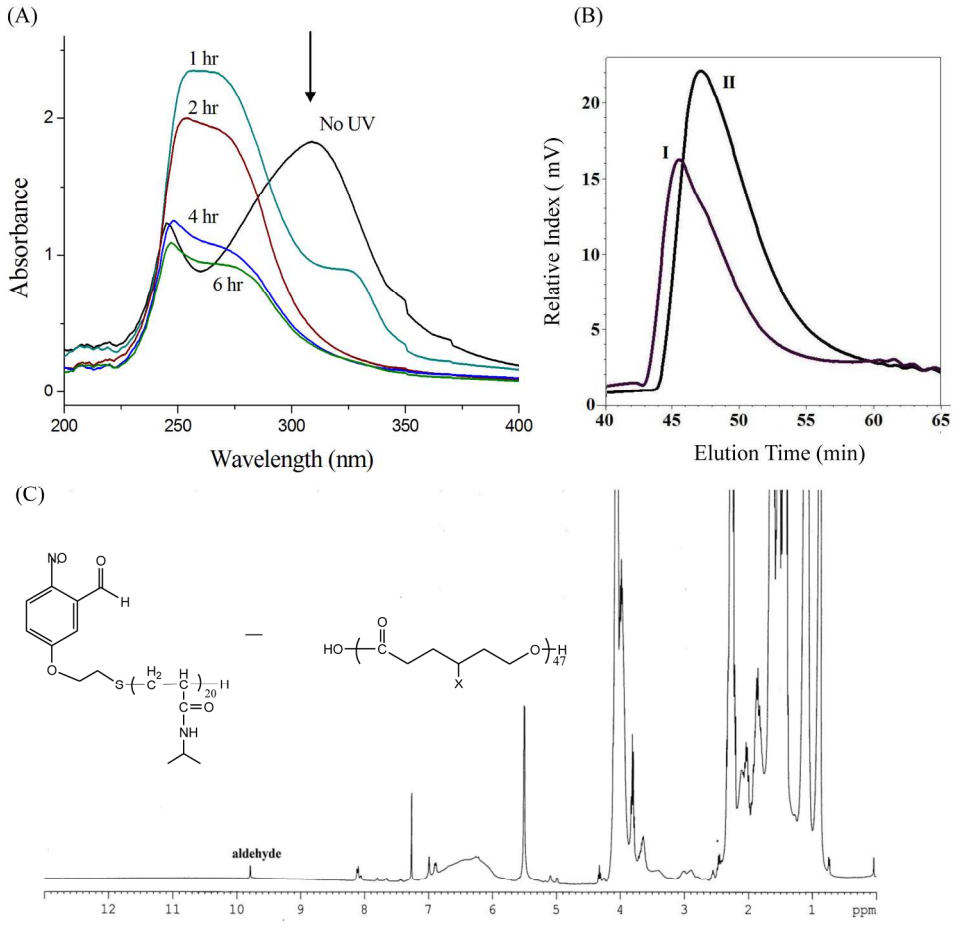

Fig. 4 (A) Time dependent UV-Vis spectra changes of $PNiPAAm_{20}$-ONB-$PMCL_{47}$ in THF (2 mg ml^{-1}), (B) GPC traces of $PNiPAAm_{20}$-ONB-$PMCL_{47}$ before (I) and after (II) UV light exposure (352 nm, 64 W) for 1 h, (C) ^{1}H NMR of $PNiPAAm_{20}$-ONB-$PMCL_{47}$ after UV irradiation for 1 h in $CDCl_3$

190x205mm (300 x 300 DPI)

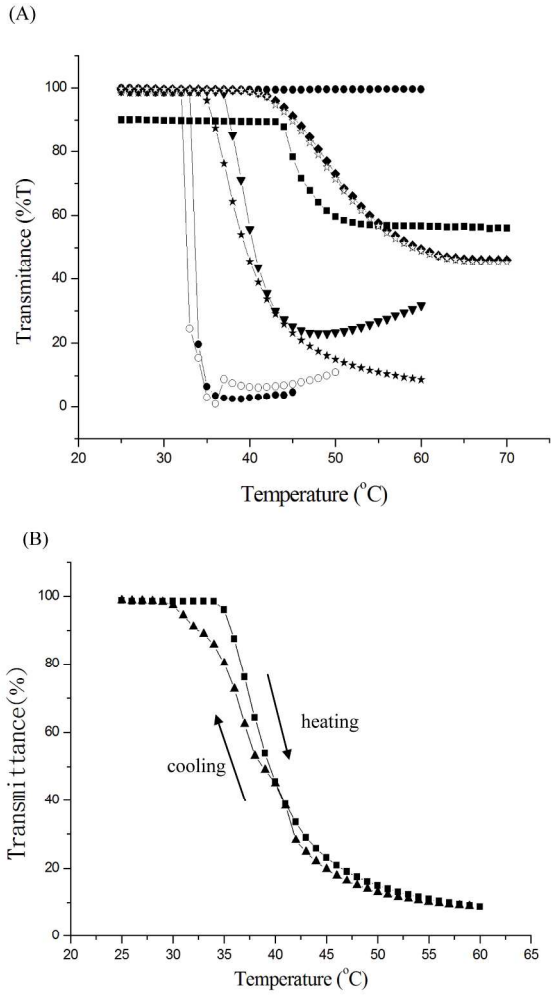

Fig. 5 (A) Phase-transition curves of (●) $PNiPAAm_{10}$-ONB-$PBCL_{55}$, (☆) $PNiPAAm_{10}$-ONB-$PMCL_{49}$, (▲) $PNiPAAm_{10}$-ONB-$PMCL_{39}$, (■) $PNiPAAm_{10}$-ONB-PCL_{12}, (▼) $PNiPAAm_{10}$-ONB-$PMCL_{13}$, (★) $PNiPAAm_{20}$-ONB-$PMCL_{49}$, (◆) $PNiPAAm_{20}$-ONB-PCL_{12}, (○) $PNiPAAm_{50}$-ONB-PCL_{12} in 0.2 wt% in DI water at λ = 500 nm, and (B) Phase-transition curves of $PNiPAAm_{20}$-ONB-$PMCL_{49}$: heating from 25 to 60 ℃ (■), and cooling from 60 to 25 ℃ (▲).

170x258mm (300 x 300 DPI)

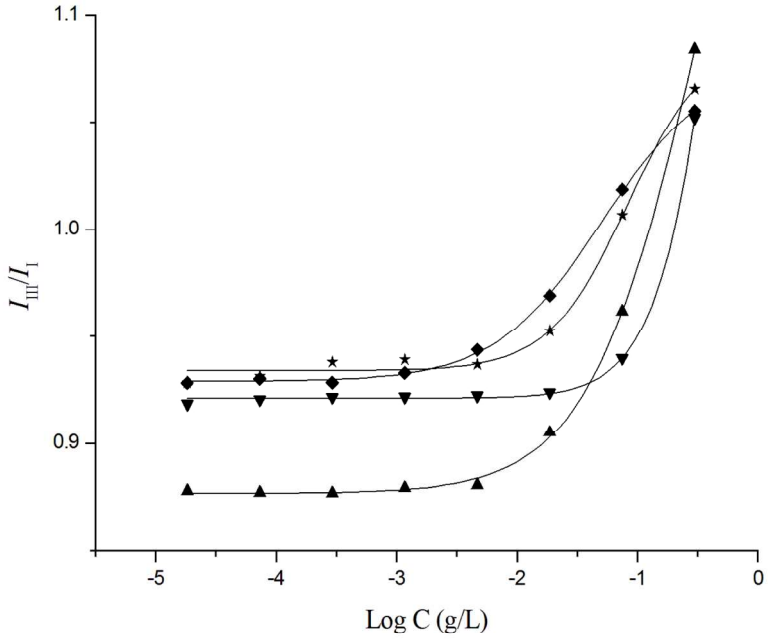

Fig. 6 Plot of I_{III}/I_I intensity ratio (from pyrene excitation spectra; pyrene concentration: (6.1×10^{-7} M) versus the logarithm of concentration (Log C) for (▼) $PNiPAAm_{10}$-ONB-$PMCL_{13}$, (▲) $PNiPAAm_{10}$-ONB-$PMCL_{39}$, (★) $PNiPAAm_{20}$-ONB-$PMCL_{49}$, and (◆) $PNiPAAm_{10}$-ONB-$PMCL_{49}$ (λ_{em} = 390 nm)

168x153mm (300 x 300 DPI)

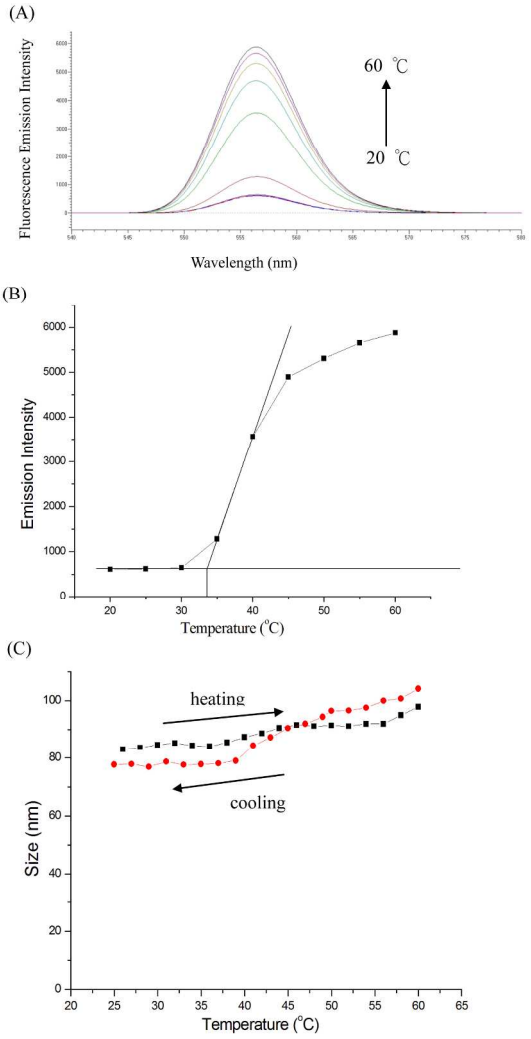

Fig. 7 Fluorescence spectra of Nile red (A) in a 0.2 wt% aqueous solution of $PNiPAAm_{20}$-ONB-$PMCL_{49}$ at temperature during the heating process, (B) the plot of maximum fluorescence intensity vs temperature, from which the critical micellization temperature (CMT) was determined, and (C) various of size as a function of solution temperature for $PNiPAAm_{20}$-ONB-$PMCL_{49}$ micelles.

157x274mm (300 x 300 DPI)

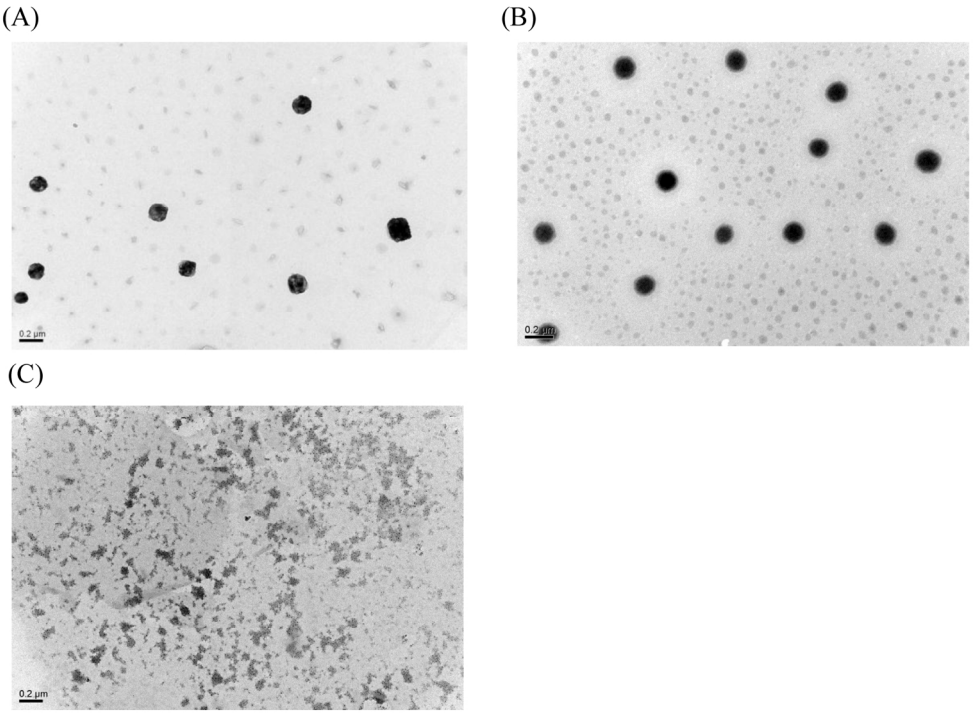

Fig. 8 TEM images of micelles formed by PNiPAAm$_{20}$-ONB-PMCL$_{49}$ (A) blank, (B) with IMC, and (C) UV irradiation for 60 s. Scale bars = 0.2 μm

157x132mm (300 x 300 DPI)

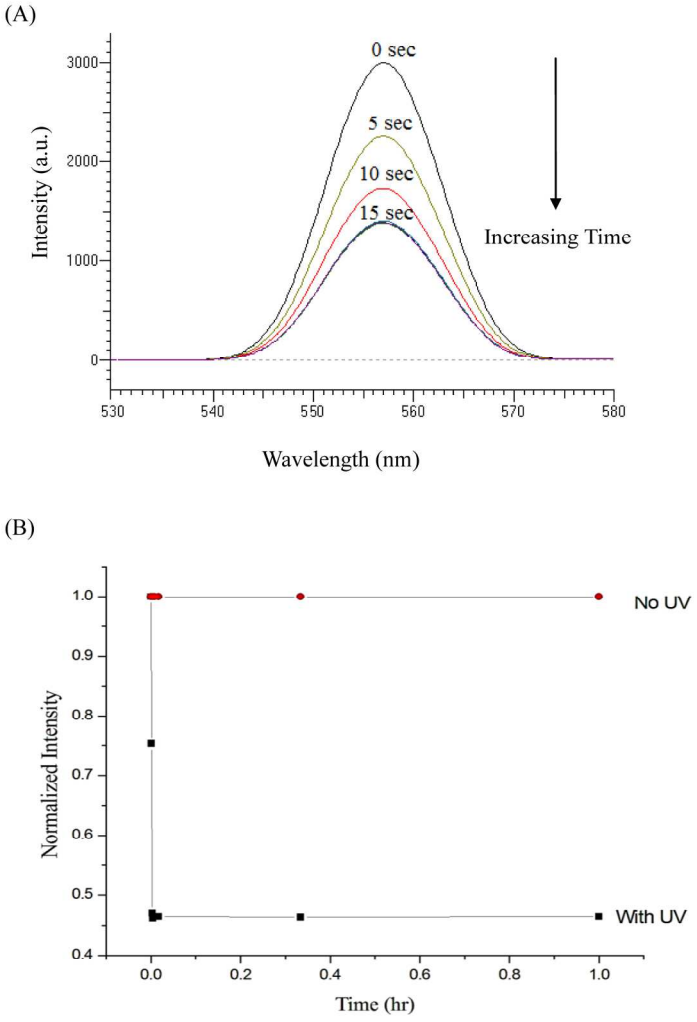

Fig. 9 (A) Fluorescence spectra of NR-loaded PNiPAAm$_{20}$-ONB-PMCL$_{49}$ micelle solution upon light irradiation (352 nm, 64 w) for 0, 5, 10, 15, 30, 60 sec and 20, 60, min.
(B) Normalized fluorescence emission intensity vs. time of the NR-loaded micelle solution with and without UV irradiation.

164x222mm (300 x 300 DPI)

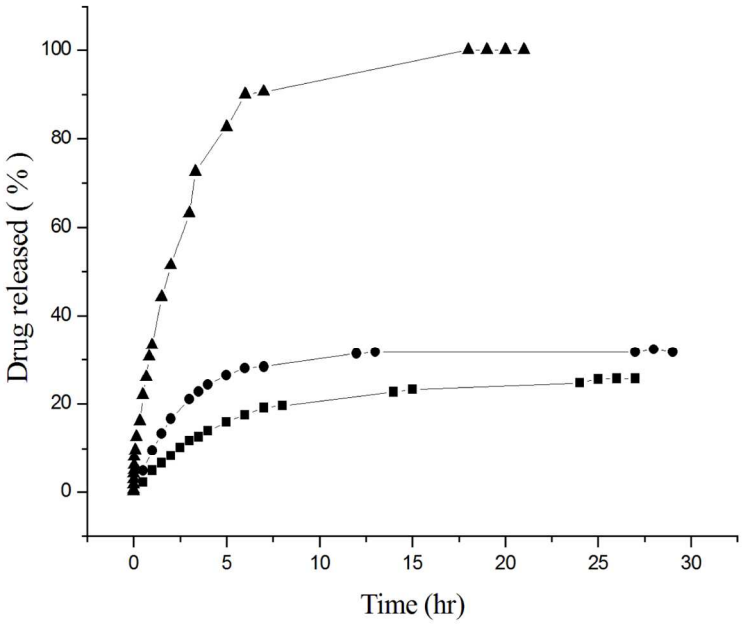

Fig. 10 IMC release from the micelle of $PNiPAAm_{20}$-ONB-$PMCL_{49}$ treated in 0.1 M PBS at different conditions: in pH 7.4 without UV irradiation at 25 ℃ (■) and 42 ℃ (●); at 42 ℃ under UV irradiation in pH 7.4 (▲).

150x128mm (300 x 300 DPI)

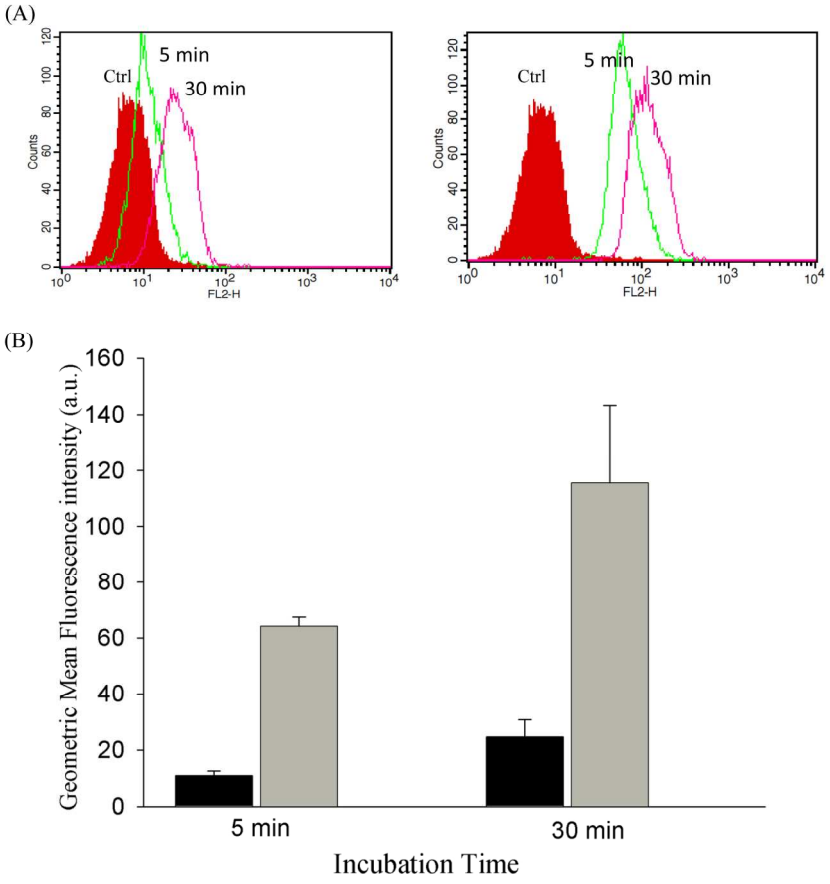

Fig. 11 (A) Flow cytometric histogram profiles of HeLa cells treated with free DOX (A, left), and DOX-loaded PNiPAAm$_{20}$-ONB-PMCL$_{49}$ (A, right) for 5 min and 30 min. Control groups were cells that did not receive any treatment, representing basal fluorescent levels. (B) Geometric mean fluorescence intensities of free DOX (black), and DOX-loaded PNiPAAm$_{20}$-ONB-PMCL$_{49}$ (gray). Data are mean ± S.E. (n = 3).

165x230mm (300 x 300 DPI)

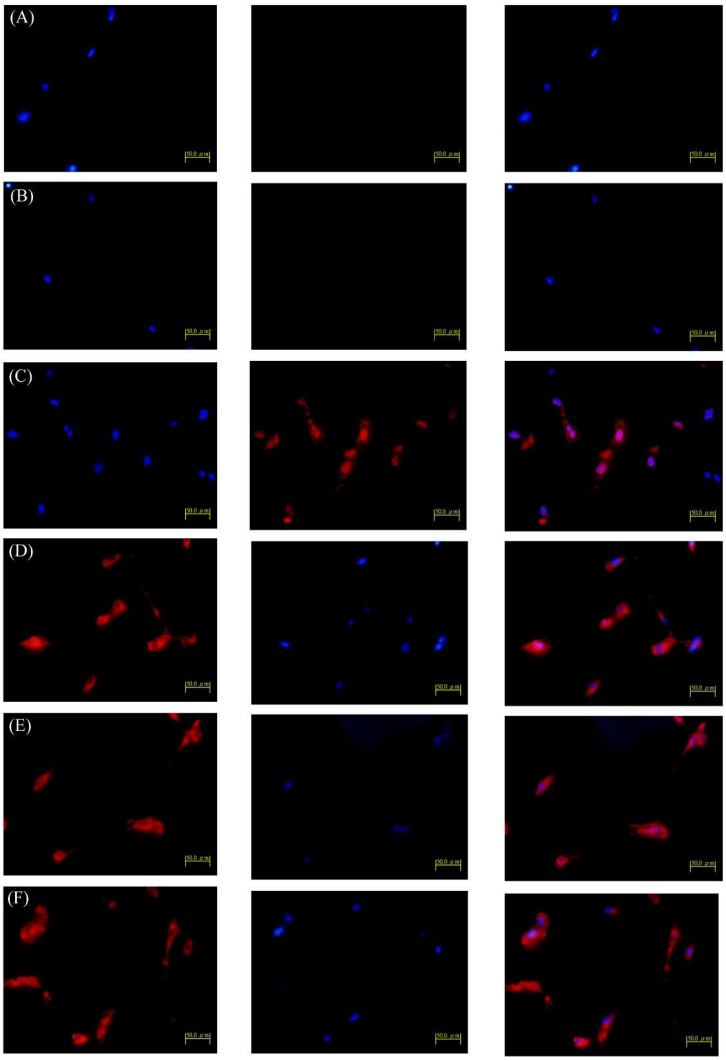

Fig. 12 Fluorescent microscopic images of HeLa cells incubated with free DOX for 5 min (A), 30 min (B) and 2 h (C), and with DOX-loaded PNiPAAm$_{20}$-ONB-PMCL$_{49}$ micelles for 5 min (D), 30 min (E) and 2 h (F). For each row, images for left to right show the cells with DOX fluorescence, Hoechst 33342 nuclear staining, and the merged image (scale bar: 50 μm; brightness not proportional to fluorescence intensity).

188x285mm (300 x 300 DPI)

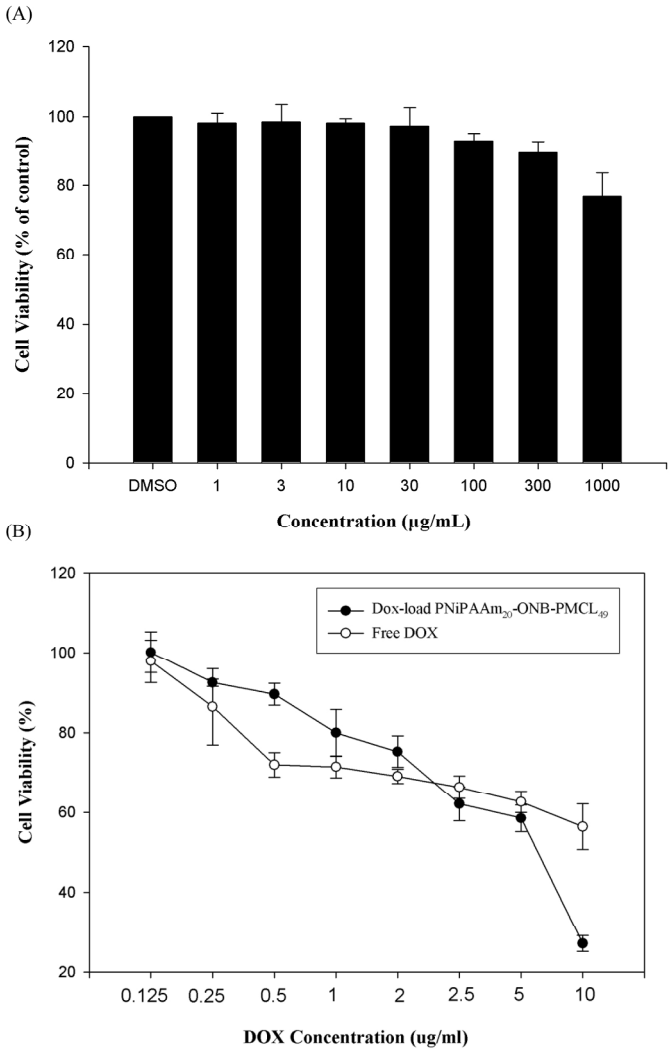

Fig. 13 The Cell viabilities of HeLa cells treated with (A) various concentrations of $PNiPAAm_{20}$-ONB-$PMCL_{49}$, (B) DOX-loaded $PNiPAAm_{20}$-ONB-$PMCL_{49}$ micelles and free DOX for 48 h, then under UV irradiation 15 sec. Data shown as mean ± S.E. (n = 3)

158x259mm (300 x 300 DPI)

Graphical abstract

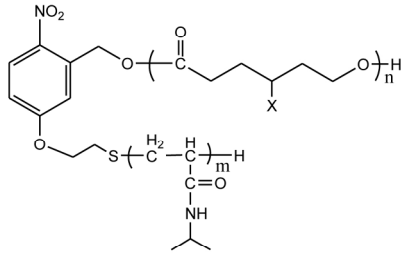

PNiPAAm-ONB-PXCL

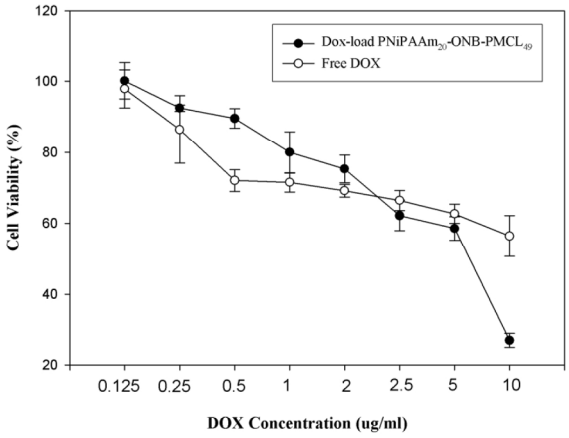

179x93mm (300 x 300 DPI)